Polylactide/Nano- and Micro-Scale Silica Composite Films. II. Melting Behavior and Cold Crystallization

Jiann-Wen Huang,[1] Yung Chang Hung,[2] Ya-Lan Wen,[3] Chiun-Chia Kang,[4] Mou-Yung Yeh[2,5]

[1]*Department of Styling & Cosmetology, Tainan University of Technology, Yung Kang, 710 Taiwan, Republic of China*
[2]*Department of Chemistry, National Cheng Kung University, Tainan, 701 Taiwan, Republic of China*
[3]*Department of Nursing, Meiho Institute of Technology, Pingtung, 912 Taiwan, Republic of China*
[4]*R&D Center, Hi-End Polymer Film Co., Ltd., Sin Ying, 730 Taiwan, Republic of China*
[5]*Sustainable Environment Research Center, National Cheng Kung University, Tainan, 701 Taiwan, Republic of China*

Received 21 July 2008; accepted 12 November 2008
DOI 10.1002/app.29699
Published online 25 February 2009 in Wiley InterScience (www.interscience.wiley.com).

ABSTRACT: Nonisothermal crystallization of polylactide (PLA)/silica composites prepared by (i) directly blending the PLA with nanoscale colloidal silica sol and by (ii) a sol–gel process are studied by differential scanning calorimeter (DSC) at various heating rates. Samples quenched from the molten state exhibited two melting endotherms (T_{ml} and T_{mh}) due to melt-recrystallization during the DSC scans. Lower heating rate and the presence of silica particles generate a lower peak intensity ratio of T_{ml} /T_{mh}. The nonisothermal crystallization kinetics is analyzed by modified Avrami model, Ozawa model, and Liu-Mo models. The modified Avrami and Liu-Mo models successfully described the nonisothermal cold crystallization processes, but Ozawa is inapplicable. The nucleation constant (K_g) is calculated by modified Lauritzen-Hoffman equation and the activation energy by Augis-Bennett, Kissinger, and Takhor models. These calculated parameters indicate consistently that the nanoscale silica particles seem to form more heterogeneous nucleation to increase crystallization, but microscale one form hindrance to retard crystallization. J Appl Polym Sci 112: 3149–3156, 2009

Key words: polylactide; silica; composite; melting behavior; cold crystallization

INTRODUCTION

Poly(lactide) (PLA) is one of the most important commercially available, synthetic biodegradable materials with sufficient mechanical properties. However, brittleness[1] and low crystallization rate[2] limit its applications. Many methods have been used to modify the physical and mechanical properties of PLA by combination with any relevant additives and/or fillers.[3–6]

Nanoscale fillers improve thermal stability, mechanical strength at low content and have thus attracted much attention. The effects of nanoscale filler on PLA nanocomposites had been reported in the literature,[7–15] such as mechanical properties, hydrolytic resistances, the thermal stability, melt behavior, mechanical properties, and so on.

The semicrystalline polymers can crystallize from the glassy and molten state, which are called glassy-crystallization and melt-crystallization, respectively. Both the physical and mechanical properties of semicrystalline polymers strongly depend on the extent of crystallization and the morphology. The fillers in polymer matrix affect not only mechanical properties but also crystallization. Studies on crystallization kinetics can realize the relationship among the processing conditions, the developed structure, and the properties of the final products.

In our previous article,[16] the PLA/silica composite films with nano- and micro-scale silica particles were prepared successfully. The particles were well dispersed in PLA, and the fillers increase the mechanical properties, thermal stability, and hydrolytical resistance. In this study, the effects of particles on the melting behaviors and the overall kinetics of the nonisothermal cold-crystallization of PLA were thoroughly investigated with differential scanning calorimetry (DSC). The experimental data were analyzed with the Avrami, Tobin, and Liu-Mo macrokinetic models. The nucleating constants were estimated by Lauritzen-Hoffman equation. The activation energy describing the nonisothermal cold-crystallization process of PLA was evaluated with Augis-Bennett, Kissinger, and Takhor models.

EXPERIMENTAL

Materials

Polylactide with a number-average molecular weight (Mn) of 206,000–207,000 was kindly provided by

Correspondence to: J.-W. Huang (jw.huang@msa.hinet.net).

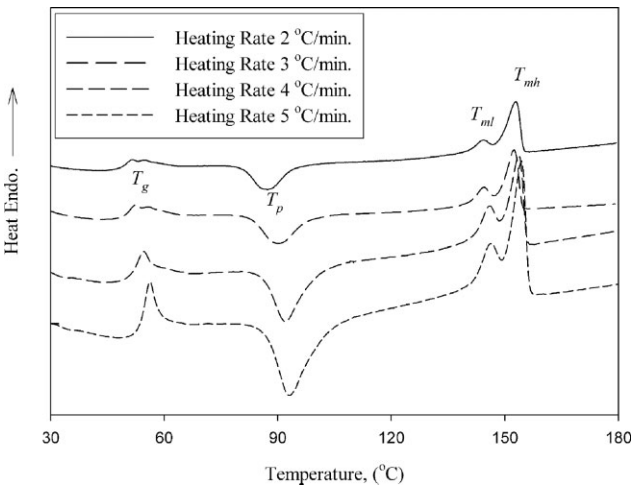

Figure 1 Melting behaviors of PLA/5col at different heating rates.

Wei Mon Industrial Co., (Taipei, Taiwan). N,*N*-Dimethylacetamide (DMAc) and tetraethoxy silane (TEOS) were purchased from Merck (Darmstadt, Germany). DMAc was dried over P_2O_5 and distilled before use. Silica sol was purchased from Nissan Chemical Co., Tokyo, Japan. The commercial product of DMAC-ST in which 20–21 wt % of silica (particle size: 10–15 nm) was dispersed in DMAc.

Preparation of PLA/silica nanocomposites

The detail preparing methods had been described in our previous article.[16] The PLA solution was prepared by dissolving PLA pellets in DMAc solution, and the solid content is 20 wt %. Two methods were used to prepare PLA/silica composite films. Method I: 5 g and 10 g of silica sol (20 wt % in DMAc) were added to 100 g of PLA solution to prepare PLA/5col and PLA/10col, respectively. The blends were cast on a releasing paper and dried at 30, 50, and 100°C in a vacuum oven. Method II: 1 g and 2 g of TEOS were added to 100 g of PLA solution with 0.1 g of 2*N* HCl to prepare PLA/5sol and PLA/10sol, respectively. The solution was mixed at room temperature for 48 h. The blends were cast on releasing paper and dried at 30, 50, and 100°C in a vacuum oven. The thickness of dry film is $\sim$ 70 μm.

Melting behaviors and nonisothermal crystallization

The melting and crystallization behaviors of polymer blends were investigated with a differential scanning calorimeter, Perkin–Elmer Pyris DSC-1. The samples were heated to 180°C and held in the molten state for 5 min to eliminate the influence of thermal history, and finally quenched in liquid nitrogen. The differential scanning calorimeter was calibrated using indium with samples weights of 8–10 mg. The sample was heated to 180°C at a heating rate (Φ) of 2, 3, 4, and 5°C/min. All operations were carried out in a nitrogen atmosphere.

RESULTS AND DISCUSSIONS

Polylactide (PLA)/silica composite films were prepared in our previous article[16] by two methods: blending of nanoscale colloidal silica sol with PLA and by a sol–gel process. The dispersion of silica particles were discussed and observed with scanning electron microscopy (SEM) and transmission electron microscope (TEM). Nano-scale particles with size 10–15 nm were well dispersed in PLA (PLA/5col and PLA/10col) by blending PLA solution with silica sol; micro-scale silica (0.8–1.2 μm for PLA/5sol and 2–3 μm for PLA/10sol) was formed from sol–gel.

Melting behavior

The representative DSC heating scan of PLA/5col at different heating rates is shown in Figure 1. The lower and higher temperature endothermic peaks are glass transition temperature (T_g) and melting temperature (T_m), respectively; the exothermic peak is attributed to the nonisothermal cold crystallization. With increasing heating rate, the endothermic traces for the cold crystallization process became wider and shifted toward higher temperatures. Table I summarized characteristic data for nonisothermal cold crystallization processes of neat PLA and PLA/silica composites. Evidently, the temperature to begin crystallization (T_0), and the temperature at the

TABLE I
Characteristic Data of Nonisothermal Cold Crystallization Exotherms for PLA and its Blends

Heating rate Φ (°C/min)		2	3	4	5
PLA	T_0 (°C)	79.8	83.2	84.1	85.9
	T_p (°C)	93.3	95.6	97.8	98.9
	$t_{1/2}$ (min)	5.15	4.10	3.52	2.92
	X_{ac} (%)	27.1	28.4	29.6	30.1
PLA/5col	T_0 (°C)	79.4	81.1	82.8	83.1
	T_p (°C)	87.3	89.9	91.9	93.0
	$t_{1/2}$ (min)	3.92	3.13	2.67	2.39
	X_{ac} (%)	19.3	20.1	21.1	21.8
PLA/10 col	T_0 (°C)	75.2	76.8	78.3	79.2
	T_p (°C)	83.1	84.9	87.1	89.9
	$t_{1/2}$ (min)	3.31	2.70	2.42	2.17
	X_{ac} (%)	18.1	18.9	19.5	20.3
PLA/5sol	T_0 (°C)	79.6	82.8	83.2	85.2
	T_p (°C)	95.1	97.9	99.1	100.9
	$t_{1/2}$ (min)	6.95	4.90	3.86	3.17
	X_{ac} (%)	21.9	22.5	23.3	24.1
PLA/10sol	T_0 (°C)	79.6	82.1	83.7	84.9
	T_p (°C)	96.1	98.6	99.5	101.7
	$t_{1/2}$ (min)	7.87	5.65	4.23	3.58
	X_{ac} (%)	21.1	21.9	22.5	23.3

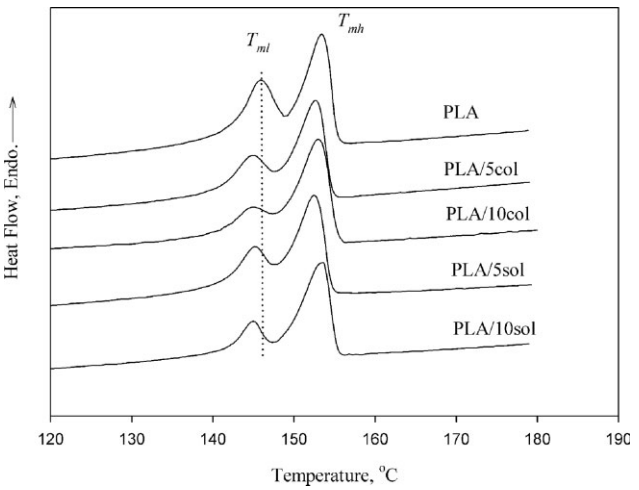

Figure 2 Multiple melting behaviors of neat PLA and PLA/silica composites at a heating rate of 4°C/min.

maximum crystallization rate (T_p) shifted toward higher temperatures with increasing heating rate.

The absolute values of crystallinity (X_{ac}) are estimated by normalized melting enthalpy (ΔH_m) and crystallization enthalpy (ΔH_c),[17,18] with the aid of the enthalpy of fusion of 93.6 J/g for the perfectly crystalline PLA.[19] The X_{ac} data are presented in Table I. At a specific heating rate, the addition of SiO_2 results in a decrease of crystallinity (X_{ac}) as a result of more defective lamella formed at the impinging interfaces. The fine SiO_2 particles form nuclei to crystallize in a limited space leading to higher proportion of interface, where the molecular chains can not be fully incorporated into growing lamella and thus form more defects in PLA matrix. Similar phenomenon has been observed in literatures.[20–22]

The melting endothermic peak splits into two peaks (T_{ml} and T_{mh}) for all heating rates. The low-temperature melting peak (T_{ml}) should be associated with the fusion of the crystals grown by normal primary crystallization, whereas the high-temperature melting endotherm (T_{ml}) related to the melting peak of the most perfect crystals after reorganization during the heating process in DSC measurement.[23]

As can be seen in Figure 1, the intensity ratio of T_{ml}/T_{mh} increase with increasing heating rate suggesting that the corresponding specimens have not enough time to complete the recrystallization (a lower intensity of T_{mh}). The results also confirm that the multiple melting is due to a mechanism based on melting and recrystallization of less perfect crystallites into thicker crystals, followed by a final melting process at higher temperature.[23,24]

Figure 2 shows the intensity ratio of T_{ml}/T_{mh} for PLA/silica composites at a specific heating rate of 4°C/min, which is lower than that of neat PLA. Silica may act as nucleating agent to promote heterogeneous nucleation, which leads to more defective crystalline in a limited space.[25] The less perfect crystalline also explains the lower T_{ml} values of PLA/silica composites than that of neat PLA. The ratio is lower for higher particle content in PLA (PLA/10col and PLA/10sol). Similar phenomenon was observed in PLA/clay.[22]

Nonisothermal crystallization

For nonisothermal crystallization, the relative degree of crystallinity, X_T, which is a function of crystallization temperature, can be defined as

$$X_T = \frac{\int_{T_0}^{T} \left[\frac{dH_c}{dT}\right] dT}{\int_{T_0}^{T_\infty} \left[\frac{dH_c}{dT}\right] dT} \quad (1)$$

where T is an arbitrary crystallization temperature at time t; T_0 and T_∞ are the initial (onset) and end of crystallization temperature, respectively. dH_c is the enthalpy of crystallization released during an infinitesimal temperature interval dT. Figure 3 present the representative relative crystallinity (X_T) as a function of temperature for PLA/5col composites. The temperature abscissa in Figure 3 could be transformed into a time scale (X_t), as shown in Figure 4, based on the following equation:[26–28]

$$t = \left|\frac{T_0 - T}{\Phi}\right| \quad (2)$$

where Φ is heating rate. It can be clearly seen from Figure 4 that the higher the heating rate, the shorter the time for completing the crystallization.

Table I also shows the half-time of crystallization ($t_{1/2}$), defined as the time from the onset of crystallization to the time at which X_t is 50%. The inverse value of $t_{1/2}$ (i.e., $1/t_{1/2}$) signifies the bulk crystallization rate and a lower $1/t_{1/2}$ value indicates slower crystallization. The $t_{1/2}$ value decreased with increasing

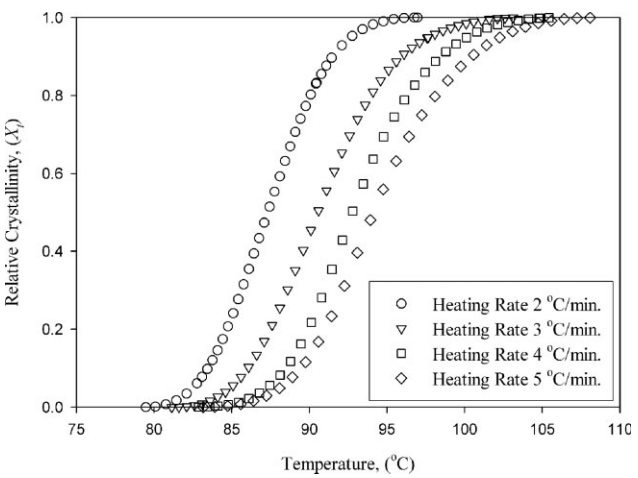

Figure 3 Experimental relative crystallinity of PLA/5col as a function of temperature at different cooling rates.

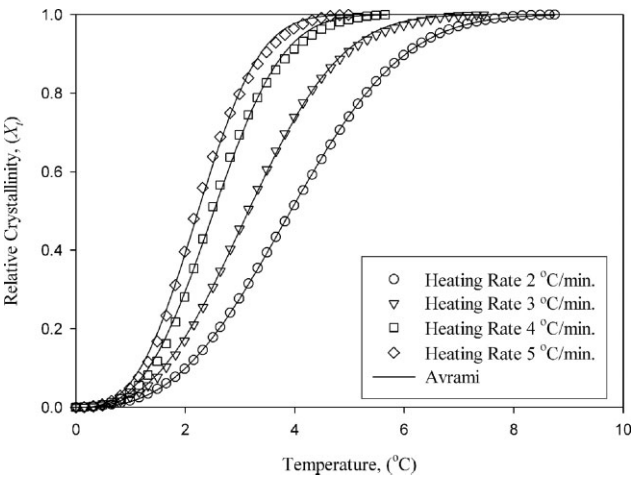

Figure 4 Experimental relative crystallinity of PLA/5col as a function of time and fitted by Avrami model at different cooling rates.

heating rate indicating the polymer crystallized faster when the heating rate was increased. The values of $t_{1/2}$ for PLA/5col and PLA/10col were evidently lower than that of neat PLA at a given heating rate, indicating that the nano-scale silica particles could accelerate the overall crystallization process. However, the values of $t_{1/2}$ for PLA/5sol and PLA/10sol increased with the addition of micron-scale silica particles. Fillers in polymer matrix usually play dual roles, as a nucleating agent to enhance crystallization and at the same time, a hindrance to retard the crystallization. The overall crystallization rate depends on the competition of these two factors. The nanoscale silica particles seem to form more heterogeneous nucleation to increase crystallization, but microscale one form hindrance to retard crystallization.

Avrami analysis

Many models have been proposed to study the nonisothermal crystallization of polymer. The most common approach is Avrami[29–31] equation. The Avrami equation is expressed as:

$$X_t = 1 - \exp(-(K_a t)^{n_a}) \quad (3)$$

where X_t is the relative crystallinity, t is crystallization time, K_a is the Avrami crystallization rate constant and n_a is the Avrami exponent. Values of K_a and n_a were found by fitting experimental data of X_t to eq. (3), and the results were shown in Table II. Because Avrami equation is based on an assumption of constant crystallization temperature, Jeziorny[32] modified the equation as following:

$$\ln K_J = \frac{\ln K_a}{\Phi} \quad (4)$$

The values of K_J were listed in Table II. K_J increased with increasing cooling rate for all samples.

The regression coefficients (R^2) in Table II indicate the Avrami equation fits the experimental data very well. The predicted curves based on the Avrami model (Fig. 4), versus the experimental; it also indicates that Avrami model provides a good and simple method to describe a nonisothermal crystallization process of neat PLA and PLA/silica composites throughout $X_t = 0$ to 1.

Avrami exponent (n_a) is related to the nucleation mechanism and crystal growth. The n_a values of neat PLA and PLA/silica composites, except PLA/10sol, are between 2.74 and 3.34, which indicate an athermal nucleation process followed by a three-dimensional heterogeneous crystal growth. The n_a value (4.10–4.26) of PLA/10sol is close to 4, which implies the crystallization proceed by thermal nucleation and three dimensional spherical growth. Although Avrami model can "describe" well the nonisothermal crystallization process of PLA and PLA/silica composites, the physical meanings of its kinetic parameters (K_a and n_a) are not so clear as isothermal crystallization because the temperature changes continually during nonisothermal crystallization process.

Ozawa analysis

Ozawa[33] assumed that a nonisothermal crystallization process may be composed of infinitesimally small isothermal crystallization steps and modified the Avrami equation to the nonisothermal case as follows:

TABLE II
Avrami Kinetics Parameters

Sample	Heating rate (K/min)	n_a	K_a	K_J	R^2
PLA	2	3.26	0.1757	0.4192	0.9998
	3	3.22	0.2164	0.6004	0.9996
	4	3.33	0.2530	0.7092	0.9997
	5	3.19	0.2658	0.7672	0.9997
PLA/5col	2	2.79	0.2235	0.4728	0.9999
	3	2.74	0.2775	0.6523	0.9998
	4	2.93	0.3500	0.7692	0.9990
	5	2.92	0.3946	0.8303	0.9990
PLA/10 col	2	3.10	0.2371	0.4869	0.9997
	3	2.83	0.3236	0.6865	0.9993
	4	2.92	0.3779	0.7841	0.9996
	5	2.82	0.4871	0.8660	0.9995
PLA/5sol	2	3.34	0.1369	0.3700	0.9991
	3	3.23	0.1856	0.5704	0.9994
	4	3.31	0.2348	0.6961	0.9990
	5	3.12	0.2533	0.7598	0.9998
PLA/10sol	2	4.26	0.1199	0.3463	0.9963
	3	4.23	0.1666	0.5502	0.9969
	4	4.10	0.2205	0.6853	0.9955
	5	4.13	0.2417	0.7528	0.9991

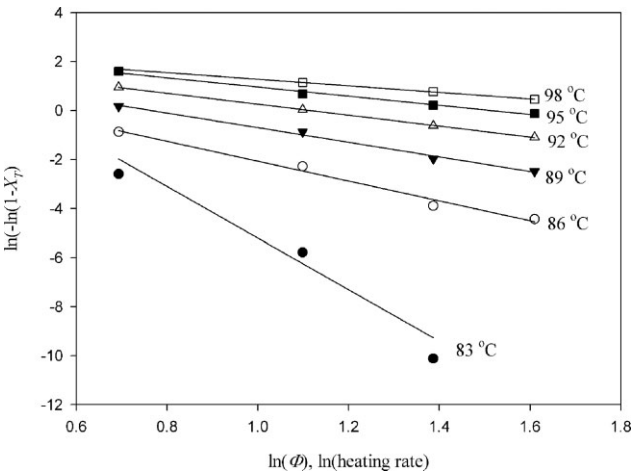

Figure 5 Ozawa analysis based on the nonisothermal cold crystallization of PLA/5col.

$$X_T = 1 - \exp\left[-\left(\frac{K_o}{\Phi}\right)^{n_o}\right] \tag{5a}$$

$$\ln\{-\ln[1 - X_T]\} = \ln K_o - n_o \ln \Phi \tag{5b}$$

Where K_o and n_o are Ozawa crystallization rate constant and Ozawa exponent, respectively. By plotting $\ln[-\ln(1 - X_T)]$ versus $\ln \Phi$ for a fixed temperature, a straight line should be obtained and the kinetic parameters, K_o and n_o, could be determined from the slope and the intercept, respectively. Figure 5 shows a typical Ozawa plots for dynamic crystallization of PLA/5col. The same trends are observed for the other samples (not shown here because of the limitation of numbers page). The Ozawa kinetic parameters as well as regression coefficient (R^2) were listed in Table III. Ozawa exponent n_o was found to range from 3.21 to 6.80 for neat PLA within 85–100°C, from 1.34 to 10.51 for PLA/5col within 83–98°C, from 0.95 to 4.22 for PLA/10col within 80–92°C, from 1.12 to 3.28 for PLA/5sol within 86–104 K and from 1.95 to 3.02 for PLA/5sol within 86–104°C. n_o increased with increasing crystallization temperature indicating the change of nucleation during the crystallization process.[34,35] The Ozawa model seems to be inapplicable for neat PLA and all PLA/silica composites.

Liu-Mo method

Liu-Mo[36] proposed a convenient kinetic method to deal with the nonisothermal crystallization by combining Avrami and Ozawa equations [eqs. (3) and (5a)]. The result is as follows:

$$\ln \Phi = \ln\left[\frac{K_o^{n_o}}{K_a^{n_a}}\right]^{\frac{1}{n_o}} - \frac{n_a}{n_o}\ln t \tag{6a}$$

$$F(T) = \left[\frac{K_o^{n_o}}{K_a^{n_a}}\right]^{\frac{1}{n_o}} \tag{6b}$$

where $F(T)$ refers to the cooling rate value, which must be chosen within unit crystallization time when the measured system amounts to a certain degree of crystallinity; a is the ratio of the Avrami exponent n_a to the Ozawa exponent n_m ($a = n_a/n_m$). A typical plot $\ln \Phi$ versus $\ln t$ (Fig. 6) yields a linear relationship between $\ln \Phi$ and $\ln t$. The data of kinetic parameter $F(T)$ and a are estimated from the intercept and slope, and the results are shown in Table IV. The a varies from 1.90 to 2.14, 1.50 to 1.61, 1.16 to 1.34, 2.04 to 2.18, and 2.20 to 2.32 for PLA, PLA/5col, PLA/10col, PLA/5sol, and PLA/10sol, respectively. The a value for each specimen is almost constant, which indicate the nonisothermal cold crystallization could be described by Liu-Mo method. The value of $F(T)$ value increases with increasing degree of crystallinity indicating that at unit crystallization time, a higher cooling rate is required to reach a higher degree of crystallinity. At a specific X_t, the $F(T)$ values of PLA/5col and PLA/10col are lower than that of neat PLA; however, those values of PLA/5sol and PLA/10sol are higher

TABLE III
Ozawa Kinetics Parameters

Sample	Temperature (°C)	n_o	K_o	R^2
PLA	85	6.80	1.311	0.9991
	88	4.67	1.508	0.9876
	91	4.01	1.939	0.9859
	94	3.71	2.469	0.9922
	97	3.51	3.085	0.9937
	100	3.21	3.747	0.9544
PLA/5col	83	10.51	1.656	0.9527
	86	4.05	1.831	0.9853
	89	2.98	2.148	0.9925
	92	2.23	3.048	0.9996
	95	1.87	4.539	0.9896
	98	1.34	7.027	0.9997
PLA/10col	80	4.22	1.442	0.99952
	83	2.93	1.733	0.9583
	86	2.26	2.652	0.9699
	89	1.76	4.206	0.9747
	92	0.95	8.769	0.9949
PLA/5sol	86	3.28	0.911	0.9917
	89	1.99	0.910	0.9220
	92	1.57	1.256	0.8952
	95	1.47	2.027	0.8909
	98	1.49	3.254	0.9009
	101	1.46	4.856	0.9280
	104	1.12	6.690	0.9449
PLA/10sol	86	3.02	0.869	0.9763
	89	2.06	0.897	0.9837
	92	1.66	1.157	0.9921
	95	1.76	1.937	0.9957
	98	2.07	3.058	0.9987
	101	2.06	4.370	0.9956
	104	1.95	6.055	0.9802

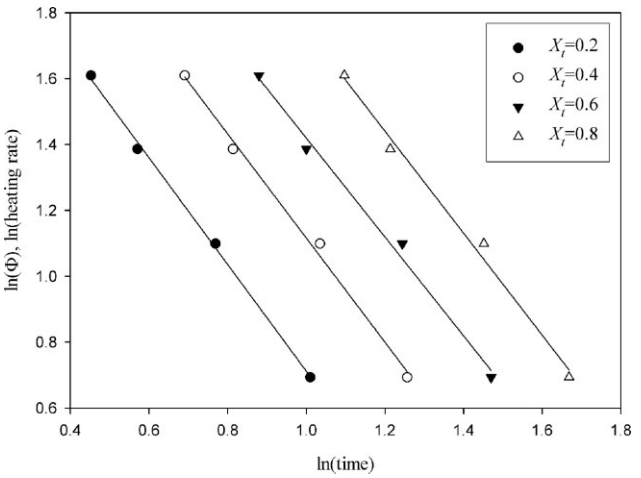

Figure 6 Plots of ln Φ versus ln(time) for different relative degrees of crystallinity for PLA/5col.

than that of neat PLA. The result also indicates that the nano-scale silica particles increase crystallization rate, but the micron-scale ones retard the process.

Inorganic fillers have been shown to play dual roles in polymer crystallization: as nuclei to enhance the crystallization, and as obstacles to retard the crystallization.[37] The nano-scale particles in PLA matrix provide more nuclei to increase the crystallization rate. On the other hand, the retarding effect overwhelms the nucleation for larger micro-scale SiO_2 and the crystallization rate is reduced

Lauritzen-Hoffman equation

Lauritzen-Hoffmann theory[37] is one of the most widely accepted theories describing the temperature dependence on the growth rate. The theory is major applied to isothermal crystallization, while Lim[38] modified the equation to be used under nonisothermal crystallization by substituting $T_c = T_o + \Phi t$. The equation is as following:

$$\ln G + \frac{U^*}{R(T_0 - \Phi t - T_\infty)} = \ln G_o - \frac{K_g}{(T_0 - \Phi t)[T_m^0 - (T_0 - \Phi t)]f} \quad (7a)$$

$$f = \frac{2(T_0 - \Phi t)}{T_m^0 + (T_0 - \Phi t)} \quad (7b)$$

G is the growth rate and is approximated as $1/t_{1/2}$ (i.e., $t = t_{1/2}$); G_o is the pre-exponential factor; U^* is the diffusional activation energy for the transport of crystallizable segments at the liquid-solid interface; R is the gas constant; $T_\infty = T_g - 30$ K is the hypothetical temperature below which viscous flow ceases and T_g is glass transition temperature of PLA. T_m^0 and T_g is 168 and 58 K, respectively[39]; K_g is the nucleation parameter which can be related to the product of lateral and folding surface free energy. Figure 7 shows the linear plot of eq. (9) for PLA and PLA/silica composites. The K_g values could be obtained from the slope of Figure 7 and follow the order: PLA/10sol > PLA/5sol > PLA > PLA/5col > PLA/10col, which indicate the crystallization ability is ranked as PLA/10col > PLA/5col > PLA > PLA/5sol > PLA/10sol. The result is in accordance with kinetic analysis.

Crystallization activation energy

The crystallization activation energy (ΔE) for nonisothermal cold crystallization process can be estimated by many models.[40–42] Considering the influence of the various heating rate in the nonisothermal cold crystallization with the peak temperature (T_p), the activation energy ΔE could be determined as following:

(1) Augis-Bennett model[40]

$$\frac{d\{\ln[\Phi/(T_0 - T_p)]\}}{d(1/T_p)} = -\frac{\Delta E}{R} \quad (8)$$

(2) Kissinger model[41]

$$\frac{d[\ln(\Phi/T_p^2)]}{d(1/T_p)} = -\frac{\Delta E}{R} \quad (9)$$

(3) Takhor model[42]

$$\frac{d[\ln(\Phi)]}{d(1/T_p)} = -\frac{\Delta E}{R} \quad (10)$$

TABLE IV
Value of *F(T)* and *a* for PLA and its Blends

Sample	X_t	$F(T)$	a	R^2
PLA	0.2	25.4	1.90	0.9597
	0.4	46.9	2.03	0.9604
	0.6	72.9	2.11	0.9735
	0.8	107.9	2.14	0.9911
PLA/5col	0.2	10.3	1.61	0.9989
	0.4	14.9	1.58	0.9951
	0.6	18.5	1.50	0.9921
	0.8	27.0	1.54	0.9914
PLA/10col	0.2	6.3	1.16	0.9942
	0.4	9.0	1.22	0.9951
	0.6	12.1	1.27	0.9937
	0.8	17.3	1.34	0.9885
PLA/5sol	0.2	31.0	2.09	0.9801
	0.4	48.2	2.04	0.9949
	0.6	80.6	2.15	0.9893
	0.8	110.5	2.18	0.9933
PLA/10sol	0.2	36.4	2.32	0.9886
	0.4	59.8	2.21	0.9792
	0.6	106.7	2.25	0.9786
	0.8	142.7	2.20	0.9732

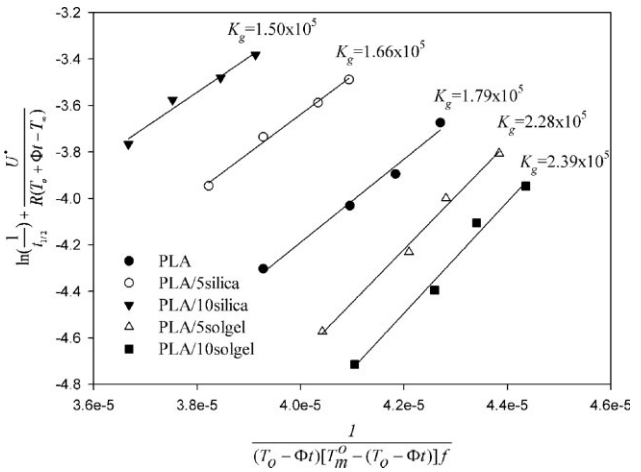

Figure 7 Determination of K_g values of neat PLA and PLA/silica composites.

where R is the universal gas constant. Figure 8(a,b) and c show the plots of Augis- Bennett model, Kissinger model and Takhor model, respectively. The activation energy ΔE can be calculated from the slopes of these plots and the results are listed in Table V. ΔE is the activation energy required to transport molecular segments to the crystallization surface. All three models show that the ΔE value of neat PLA is lower than those of PLA/5sol and PLA/10sol, but higher than those of PLA/5col and PLA/10col. The results further provide evidences to show that the crystallization rate can be increased and reduced by nano- and micro-scale silica particles, respectively.

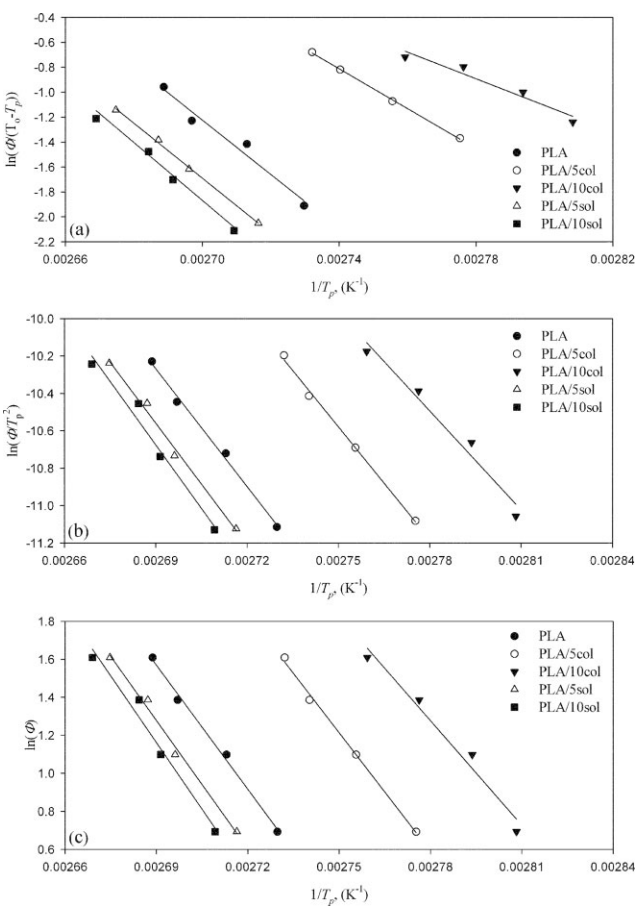

Figure 8 Determination of the crystallization activation energy for PLA/5col. (a) Augis-Bennett model, (b) Kissinger model, and (c) Takhor model.

TABLE V
Crystallization Activation Energy ΔE (kJ/mole) Calculated from Augis-Bennett, Kissinger, Takhor Models

Samples	X_t	Augis-Bennett	Kissinger	Takhor
PLA	ΔE	181.0	174.6	180.7
	R^2	0.9681	0.9953	0.9953
PLA/5sol	ΔE	159.8	166.8	172.8
	R^2	0.9991	0.9969	0.9969
PLA/10sol	ΔE	88.6	146.5	152.5
	R^2	0.9982	0.9708	0.9723
PLA/5sol	ΔE	183.2	180.5	186.7
	R^2	0.9990	0.9954	0.9957
PLA/10sol	ΔE	192.8	188.1	194.4
	R^2	0.9926	0.9899	0.9921

CONCLUSIONS

Melting behavior and nonisothermal crystallization of polylactide/silica composites are studied by DSC. DSC scans for samples quenched from the molten state exhibited two melting endotherms (T_{ml} and T_{mh}), resulting from the melt-recrystallization process during the DSC scans. Higher heating rate allows less time to complete the recrystallization and results in a higher intensity ratio of T_{ml}/T_{mh}. The presence of silica induces more nuclei to crystallization from molten state and lead to more crystalline defects, which results in a lower intensity ratio of T_{ml}/T_{mh}. The cold nonisothermal crystallization is described successfully by modified Avrami and Liu model. The nanoscale silica particles promote heterogeneous nucleation to increase crystallization, but microscale one form hindrance to retard crystallization. The nucleation constant (K_g) that is calculated by modified Lauritzen-Hoffman equation and the activation energy estimated by Augis-Bennett, Kissinger, and Takhor models further support the results.

References

1. Ikada, Y.; Tsuji, H. Macromol Rapid Commun 2000, 21, 117.
2. Tsuji H. In Recent Research Developments in Polymer Science; Pandalai, S. G., Ed.; Transworld Research Network: Trivandrum, India, 2000; Vol. 4, p 13.
3. Drumright, R. E.; Gruber, P. R.; Henton, D. E. Adv Mater 2000, 12, 1841.

4. Sodergard, A.; Stolt, M. Prog Polym Sci 2002, 27, 1123.
5. Auras, R.; Harte, B.; Selke, S. Macromol Biosci 2004, 4, 835.
6. Mecking, S. Angew Chem Int Ed 2004, 43, 1078.
7. Ray, S. S.; Maiti, P.; Okamoto, M.; Yamada, K.; Ueda, K. Macromolecules 2002, 35, 3104.
8. Ray, S. S.; Maiti, P.; Okamoto, M.; Yamada, K.; Ueda, K. Polymer 2003, 44, 857.
9. Nam, P. H.; Fujimori, A.; Masuko, T. J Appl Polym Sci 2004, 93, 2711.
10. Wu, L.; Cao, D.; Huang, Y.; Li, B. G. Polymer 2008, 49, 742.
11. Yan, S. F.; Yin, J. B.; Yang, Y.; Dai, Z. Z.; Ma, J.; Chen, X. S. Polymer 2007, 48, 1688.
12. Paul, M. A.; Alexandre, M.; Degee, P.; Calberg, C.; Jerome, R.; Dubois, P. Macromol Rapid Commun 2003, 24, 561.
13. Pluta, M.; Galeski, A.; Alexandre, M.; Paul, M. A.; Dubois, P. J Appl Polym Sci 2002, 86, 1497.
14. Chang, J. H.; An, Y. U.; Sur, G. S.; J Polym Sci Part B: Polym Phys 2003, 41, 94.
15. Ogata, N.; Jimenez, G.; Kawai, H.; Ogihara, T. J Polym Sci Part B: Polym Phys 1997, 35, 389.
16. Huang, J. W.; Hung, Y. C.; Wen, Y. L.; Kang, C. C.; Yeh, M. Y. J Appl Polym Sci, accepted.
17. Li, S.; McCarthy, S. Macromolecules 1999, 32, 4454.
18. Zhao, Y. L.; Cai, Q.; Jiang, J.; Shuai, X. T.; Bei, J. Z.; Chen, C. F.; Xi, F. Polymer 2002, 43, 5819.
19. Fischer, E. W.; Sterzel, H. J.; Wegner, G. Kolloid Z. Z. Polymer 1973, 251, 980.
20. Tjong, S. C.; Bao, S. P. J Polym Sci Part B: Polym Phys 2004, 42, 2878.
21. Wu, D. F.; Zhou, C. X.; Xie, F.; Mao, D. L.; Zhang, B. J Appl Polym Sci 2006, 99, 3257.
22. Wu, D.; Wu, L.; Wu, L.; Xu, B.; Zhang G, Y.; Zhang, M. J Polym Sci Part B: Polym Phys 2007, 45, 1100.
23. Liu, X.; Li, C.; Zhang, D.; Xiao, Y. J Polym Sci Part B: Polym Phys 2006, 44, 900.
24. Nichols, M. E.; Robertson, R. E. J Polym Sci: Polym Phys Ed 1992, 30, 755.
25. Gao, J.; Wang, D.; Yu, M.; Yao, Z. J Appl Polym Sci 2004, 93, 1203.
26. Hay, J. N.; Sabir, M. Polymer 1969, 10, 203.
27. Hay, J. N.; Fitzgerald, P. A.; Wiles, M. Polymer 1976, 17, 1015.
28. Hay, J. Br Polym J 1979, 11, 137.
29. Avrami, M. J Chem Phys 1939, 7, 1103.
30. Avrami, M. J Chem Phys 1940, 8, 212.
31. Avrami, M. J Chem Phys 1941, 9, 177.
32. Jeziorny, A. Polymer 1978, 19, 1142.
33. Ozawa, T. Polymer 1971, 12, 150.
34. Qiu, Z.; Fujinami, S.; Komura, M.; Nakajima, K.; Ikehara, T.; Nishi, T. Polym J 2004, 36, 642.
35. Somrang, N.; Nithitanakul, M.; Grady, B. P.; Supaphol, P. Eur Polym J 2004, 40, 829.
36. Liu, T. X.; Mo, Z. S.; Wang, S. E.; Zhang, H. F. Polym Eng Sci 1997, 37, 568.
37. Hoffman, J. D.; Davis, G. T.; Lauritzen J. I. In Treatiseon Solid State Chemistry; Hannay, N. B., Ed.; Plenum: New York, 1976, p 3.
38. Lim, G. B. A.; Mcguire, K. S.; Lloyd, D. R. Polym Eng Sci 1993, 33, 537.
39. Nam, J. Y.; Ray, S. S.; Okamoto, M. Macromolecules 2003, 36, 7126.
40. Augis, J. A.; Bennett, J. E. J Therm Anal 978, 13, 283.
41. Kissinger, H. E. J Res Nat Bur Stand 1956, 57, 217.
42. Takhor, R. L. Advances in Nucleation and Crystallization of Glasses; American Ceramics Society: Columbus, 1971, p 166.